6 Very High Energy Gamma Ray Astronomy with CTA

D. Florin, A. Gadola, R. Gredig, B. Huber, A. Manalaysay, S. Steiner, U. Straumann, A. Vollhardt

in collaboration with: University of Geneva, EPFL Lausanne, ETH Zürich, Jagiellonian University Cracow, MPI für Kernphysik Heidelberg, University of Leeds, Universität Tübingen.

The full CTA collaboration consists of 115 institutes from 23 countries.

(CTA)

The Cherenkov Telescope Array (CTA) is a planned next generation array of Imaging Atmospheric Cherenkov Telescopes (IACTs), and is the successor to the current generation of IACTs including MAGIC [1], H.E.S.S [2], and VERITAS [3]. These telescopes are used to detect Very High Energy (VHE) gamma ray photons, in the range of tens of GeV to tens of TeV, emitted from exotic (i.e. non-thermal) astrophysical sources such as quasars, supernovae and their remnants, gamma-ray bursts, and dark matter annihilations. When these gamma rays enter the Earth's upper atmosphere, they are converted to an electron-positron pair, with the two particles together sharing the energy of the parent gamma ray. The electron and positron trigger an electromagnetic shower containing many highly-energetic charged particles. Many of these particles travel at speeds exceeding the speed of light in the atmosphere, and as a result produce Cherenkov photons that travel in a cone to the ground. The IACTs detect these Cherenkov photons and can reconstruct the structure of the electromagnetic shower by viewing the shower from multiple telescopes, and by analyzing the time structure of the photon arrival times. The reconstructed electromagnetic shower can then be used to determine the direction and energy of the initial gamma ray that was incident upon the upper atmosphere.

CTA is currently in a phase of heavy research and development. The goal is not to build larger versions of the current IACTs arrays listed above, but to build *improved* versions based upon lessons learned from current experience, and also by exploiting new technologies that have arisen in the years since the current IACTs were designed. Efforts at UZH towards this goal include modular and distributed clock generation techniques (see Sec. 18), primary mirror alignment,optical components of the first Geiger-mode Avalanche Photodiode IACT camera, and a first fully-digital IACT camera.

6.1 Mirror tracking

The primary mirror of these telescopes is made up of many individual mirror segments. Our group is designing a fast and reliable tracking system that orients the individual mirror segments with an accuracy that fits the severe optical quality requirements.

The system makes use of a standard digital (CMOS) camera situated in the focal plain of the telescope. While the telescope is pointing to a bright light source (e. g. a star) the orientation of each mirror segment is optimised by maximizing apparent brightness of the mirror image.

To analyze the optical behavior and determine the prerequisites to align an entire telescope, a simulation-tool has been developed that is able to control parameters like the mirror PSF, mirror orientation, lens orientation/position and light source intensity. The resulting camera view can also be simulated (Fig. 6.1). With the help of this simulation the response can be estimated when a certain parameter is changed.

A test setup has been built at the UZH to optimize the alignment algorithm and test the camera usage.

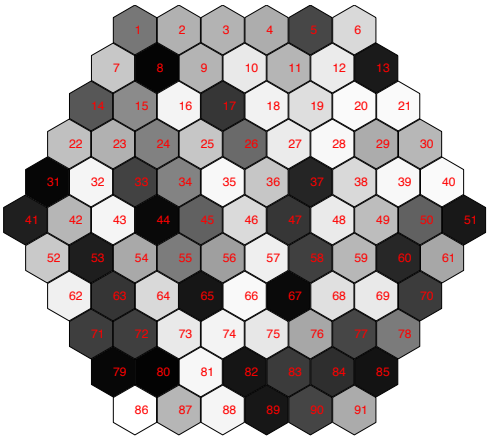

Fig. 6.1 – Example of a CTA-like telescope simulation with a camera in the focal plain and randomly aligned mirrors. Each hexagon represents an individual mirror segment.

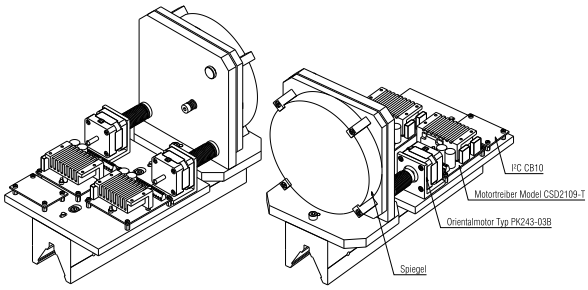

Fig. 6.2 – Schematics of the mirror mount.

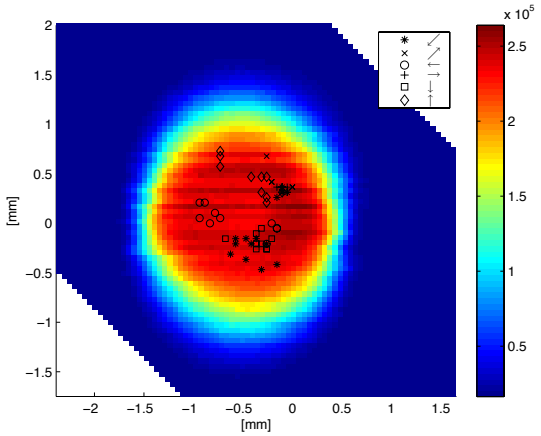

Fig. 6.3 – Results of a simulation cycle showing the illumination intensity of the camera depending on the mirror orientation (a. u.). The black symbols show the position found by the algorithm after displacing the mirror in the direction indicated by the arrows.

A spherical mirror of 6 inch diameter with a focal length of 1.5 m is installed on a mount where the tilt can be adjusted with the help of three positioning screws. Two of these screws are connected to stepping motors (Fig. 6.2) controlled by a complete embedded computer connected through a I^2C bus to the camera and capable of executing the scan algorithm. The system has been successfully tested and can deal with a noisy source or with a temporary blackout. For this test the light from an antenna-tower at about 2 km distance has been used as a light source. Figure 6.3 shows an example of the camera's response to different mirror positions. The optimal positions found by the algorithm while realigning the mirror are also shown.

6.2 Light concentrators for the FACT camera

Light incident on the telescope's primary mirror is reflected towards the mirror's focal plane where the pixelized camera is located. The desired field of view of the telescope which extends typically 1.5 to 2 m sets the scale of the camera. It is not practical to completely cover this area with photosensors. Instead, the single pixels are equipped with light concentrators which results in an almost full coverage. Current imaging air Cherenkov telescopes, like HESS and MAGIC, use compound parabolic concentrators, so-called Winston cones. They have a hollow body covered with reflective foils at the inner walls and are combined with photomultiplier tubes as photosensors. The CTA Group at UZH, in close cooperation with ETH Zurich, has contributed extensively to the development of parabolic solid light concentrators which make use of total internal reflection. These are made of injection-moulded polymethyl methacrylate and interface a hexagonal entrance to a square exit area tailored to the sensitive area of novel commercial 3x3 mm^2 Geiger-mode avalanche photodiodes (GAPD) (see. Fig. 6.4) which so far have not been used in IACTs. The increased areal

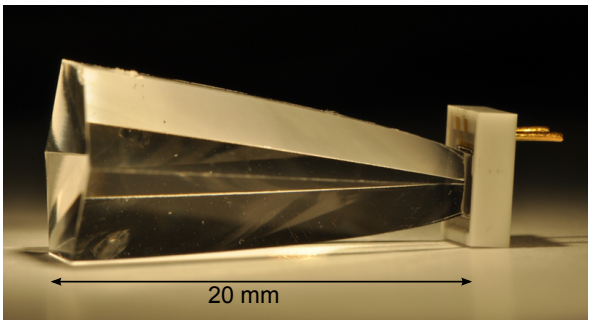

Fig. 6.4 – A light concentrator optically glued to a GAPD. The length of the concentrator is 20 mm. The 2.8x2.8 mm^2 exit area matches the GAPD's sensitive area of 3x3 mm^2.

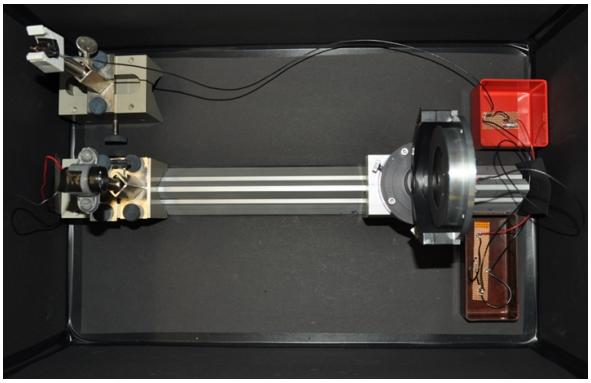

Fig. 6.5 – Top view of the goniometer test setup built to quantify the performance of the light concentrators.

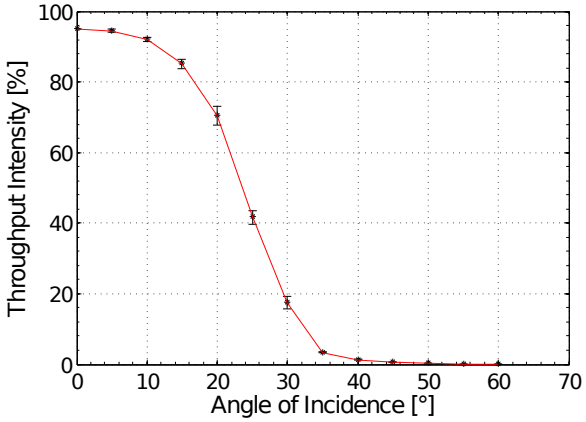

Fig. 6.6 – The light transmission of the light concentrator as a function of the zenith angle of incident photons. The shaded area indicates the angles subtended by the primary mirror.

acceptance can only be achieved at the cost of a reduced angular acceptance (see Fig. 6.6) which, in fact, is an advantage since which is effectively cut at $\sim 20°$ with the advantage of drastically reducing the sensitivity to stray photons from the night sky.

A test setup has been built at UZH (Fig. 6.5) which includes a light source providing almost parallel light and a goniometer in which a set of five light concentrators can be placed. The setup offers the possibility to measure light transmission through the concentrator at a fixed wavelength and vertical incidence, to characterize the angular response and to study optical cross talk between neighboring devices. In Fig. 6.6, the light throughput as a function of the zenith angle of incident rays is plotted as measured by this test setup.

6.3 FlashCam preamplifiers

FlashCam aims at building the first fully-digital IACT camera. Our efforts are two-fold: development of a non-linear preamplifier designed for increased dynamic range of the photomultiplier tubes, and design of the camera triggering system.

Photomultiplier tubes (PMT) are used in the telescope's camera to detect Cherenkov light. A low PMT gain of about 40'000 is required to slow down aging and increase the lifetime beyond ten years. The resulting very small output signals for single photoelectrons (phe) need to be amplified. Such amplification stage must have an excellent signal to noise ratio and a good amplitude resolution over a large dynamic range of up to 3'000 phe. The large dynamic range is normally covered by two parallel signal channels with different amplifications. Alternatively, a non-linear amplifier could be used connected to a single readout channel only. A non-linear amplification can be achieved, for example, by driving an operational amplifier (opamp) into saturation, but maintaining the charge (so increasing the signal width). The design shown in Fig. 6.7 with the current feedback opamp AD8001 satis-

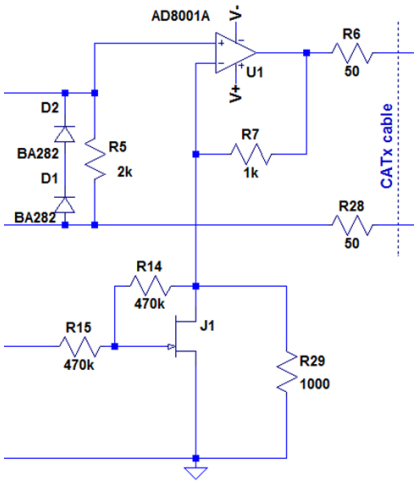

Fig. 6.7 – Amplfier circuitry using the AD8001 opamp. Input is on the upper left. The pseudo-differential output is transmitted through a CAT 5 cable to the FADC. The lower part of the circuit with the J-FET is used to set the gain.

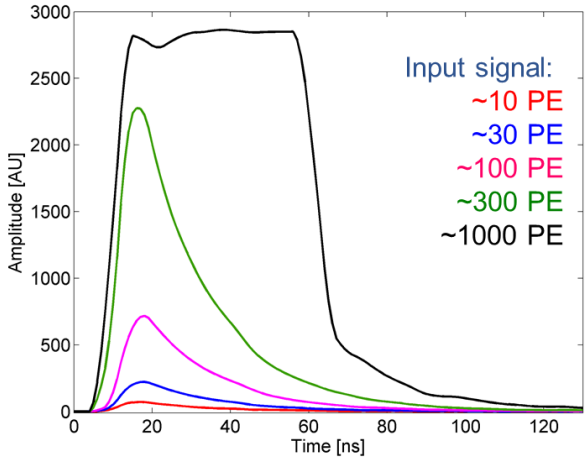

Fig. 6.8 – Digitized signals of different amplitudes. The saturation of the opamp is clearly visible for the 1000 phe pulse. The 300 phe pulse shows as well some saturation which is hardly recognizable for the untrained eye.

fies our requirements. The opamp has two distinct saturation modes: saturation caused by a large input signal, and saturation caused by driving the opamp's output signal beyond its output range. The first saturation mode causes ringing and is therefore not desired. A simple diode in the input circuit limits the input signal and prevents the opamp to saturate. The second mode can be achieved by the selected gain. This allows also setting the point between the linear and non-linear region. A set point of about 200 phe is chosen for our purpose.

Figure 6.8 shows digitized PMT pulses in the linear and in the saturation region. The original amplitude is determined by summing the signal over time window of 200 ns. This scheme can cope with high background levels (several incident photons during 10 ns) of low amplitude signals (< 10 phe).

Further studies with the amplifier will be performed and a first prototype board for the FlashCam with twelve PMTs and amplifiers will be built. Studies on the signal reconstruction are planned as well.

6.4 FlashCam trigger

The FADC outputs are passed to a Field-programmable Gate Array (FPGA). The FPGA stores the data in a digital ring buffer and performs a preliminary data reduction combining the signals from groups of three or seven neighbours to be presented to the trigger logic that initiates the readout of the associated FPGA information over Ethernet to a central server. FPGA-based triggering schemes offer much greater flexibility compared to the present analog systems. A good trigger algorithm must distinguish shower events from diffuse night sky background with high sensitivity over a wide range of energies and with good uniformity across the camera area.

The performance of trigger algorithms is assessed by Monte Carlo simulations which provide the "effective area" of the telescope. A *digital majority* requires a minimal number of signals above a certain amplitude threshold. This basic algorithm is used as a benchmark. *Digital sum* algorithms utilize the total amplitude of groups of pixels which improves the trigger uniformity. The effective areas, as a function of gamma ray energy, of these

two triggering algorithms are shown in Fig. 6.9.

The performance of various triggering algorithms is assessed by Monte Carlo simulations. These simulations can be used to determine many properties of the triggering algorithm, the most important being the "effective area" of the telescope which measures the area of the Earth's atmosphere from which gamma ray Cherenkov showers can be detected in a single telescope. The *digital majority* algorithm requires a minimal number of pixels having signals above a variable threshold. This basic algorithm is used as a benchmark. *Digital sums* form an alternative class of trigger algorithms which use the combined amplitude information over groupings of pixels to distinguish real showers from night sky background photons. The effective area, as a function of gamma ray energy, of one type of digital sum trigger is shown in Fig. 6.9. It would be very hard to implement such complex algorithm in the hardware-based triggers that are commonly used at present.

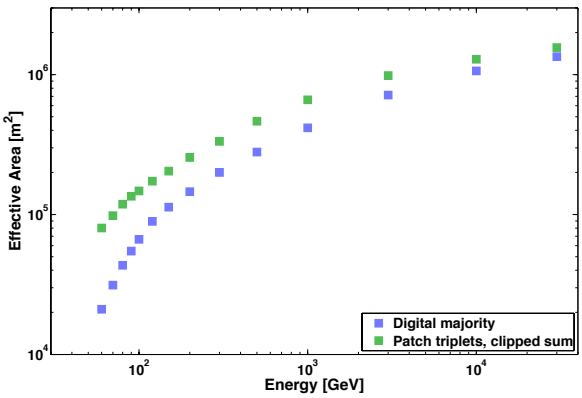

Fig. 6.9 – The effective collection area of a single telescope as a function of gamma ray energy, for two trigger algorithms (see text).

[1] J. A. Coarasa *et al.* (MAGIC Collaboration), J. Phys. Soc. Jap. Suppl **77B**, 49 (2008).

[2] B. Opitz *et al.* (HESS Collaboration), AIP Conf. Proc. **1223** 140 (2010).

[3] D. Hanna *et al.* (VERITAS Collaboration), J. Phys. Conf. Ser. **203** 012118 (2010).